Spin Dynamics and Phonons in Chromites $CoCr_2O_4$ and $MnCr_2O_4$

Spin Dynamics and Phonons in Chromites $CoCr_2O_4$ and $MnCr_2O_4$

Wei Xu(徐威)[1], Gaoting Lin(林高庭)[1], Mingfang Shu(舒明方)[1], Jinlong Jiao(焦金龙)[1], Jinfeng Zhu(朱金峰)[1], Qingyong Ren(任清勇)[2,3,4], Manh Duc Le[5], Xuan Luo(罗轩)[6], Yuping Sun(孙玉平)[6,7,11], Yi Liu(刘毅)[8], Zhe Qu(屈哲)[7], Haidong Zhou(周海东)[9], Shang Gao(高尚)[10], and Jie Ma(马杰)[1,11*]

[1]*Key Laboratory of Artificial Structures and Quantum Control, School of Physics and Astronomy, Shanghai Jiao Tong University, Shanghai 200240, China*
[2]*Institute of High Energy Physics, Chinese Academy of Sciences, Beijing 100049, China*
[3]*Spallation Neutron Source Science Center, Dongguan 523803, China*
[4]*Guangdong Provincial Key Laboratory of Extreme Conditions, Dongguan 523803, China*
[5]*ISIS Neutron and Muon Source, STFC Rutherford Appleton Laboratory, Didcot OX11 0QX, United Kingdom*
[6]*Key Laboratory of Materials Physics, Institute of Solid State Physics, Chinese Academy of Sciences, Hefei 230031, China*
[7]*Anhui Province Key Laboratory of Condensed Matter Physics at Extreme Conditions, High Magnetic Field Laboratory, Chinese Academy of Sciences, Hefei 230031, China*
[8]*National Synchrotron Radiation Laboratory, University of Science and Technology of China, Hefei 230026, China*
[9]*Department of Physics and Astronomy, University of Tennessee, Knoxville 37996, USA*
[10]*Department of Physics, University of Science and Technology of China, Hefei 230026, China*
[11]*Collaborative Innovation Center of Advanced Microstructures, Nanjing University, Nanjing 210093, China*

(Received 16 August 2024; accepted manuscript online 10 October 2024)

Spinel compounds are of great interest in both fundamental and application-oriented perspectives due to the geometric magnetic frustration inherent to their lattice and the resulting complex magnetic states. Here, we applied x-ray diffraction, magnetization, heat capacity and powder inelastic neutron scattering measurements, along with theoretical calculations, to study the exotic properties of chromite-spinel oxides $CoCr_2O_4$ and $MnCr_2O_4$. The temperature dependence of the phonon spectra provides an insight into the correlation between oxygen motion and the magnetic order, as well as the magnetoelectric effect in the ground state of $MnCr_2O_4$. Moreover, spin-wave excitations in $CoCr_2O_4$ and $MnCr_2O_4$ are compared with Heisenberg model calculations. This approach enables the precise determination of exchange energies and offers a comprehensive understanding of the spin dynamics and relevant exchange interactions in complicated spiral spin ordering.

DOI: 10.1088/0256-307X/41/11/117503

As a typical three-dimensional (3D) geometric frustration family, spinel system, AB_2O_4, exhibits a series of exotic physical properties not only from the variation of cations on tetrahedrally (A) and octahedrally (B) coordinated sites,[1–5] but also the geometric-frustrating B-site cations with a pyrochlore sublattice. Hence, the spinel materials could host diverse magnetic behaviors, ranging from ferrimagnetism to antiferromagnetism, depending on the nature of the cations and their interactions.[6–8] Actually, the magnetic properties of spinel compound are decided by whether the A- and B-site cations are magnetic or nonmagnetic: if both A- and B-site cations are magnetic, the complicated interactions of A–A, B–B, and A–B could display intriguing physics. For instance, the vanadate AV_2O_4 is an orbiton family where the B-site V^{3+} ions can introduce orbital ordering with complex magnetic ordering and structural distortions.[7,9–12]

Chromium-based spinel ACr_2O_4 (where A is a divalent $3d$ transition metal) is of significant interest as the Cr^{3+} ions ($3d^3$ with $t_{2g}^3e_g$) lack orbital degeneracy and provides a clearer view of the underlying Heisenberg magnetic-exchange interactions.[13] A representative example is the nonmagnetic A-site compound $ZnCr_2O_4$, which has a highly frustrated ground state on the pyrochlore sublattice from the nearest-neighbor (NN) antiferromagnetic (AFM) exchange interactions ($J_{\mathrm{Cr-Cr}}$) between Cr^{3+} cations. This system can realize a cooperative paramagnet with cluster-like scattering over a wide temperature range of $T_{\mathrm{N}} < T < |\theta_{\mathrm{CW}}|$, where T_{N} is the magnetic ordering temperature and θ_{CW} is the Curie–Weiss temperature. However, an exotic complex spin order emerges below $T_{\mathrm{N}} \sim 12.5\,\mathrm{K}$, accompanied by a structural distortion to a tetragonal phase.[14,15] The microscopic mechanism of this phase transition may be attributed to the combined effects of NN and further-neighbor (FN) Heisenberg interactions, spin-lattice coupling, and asymmetric magnetic interactions.

If the A-site cation is magnetic, such as Co^{2+} or Mn^{2+},

*Corresponding author. Email: jma3@sjtu.edu.cn

a tetragonal-cubic transition is not observed, while the complex spin ordering has been exhibited. In the early 1960s, Lyons, Kaplan, Dwight, and Menyuk (LKDM) proposed a theoretical model to understand this complex spin order under the cubic structure.[16] Due to the occupation of magnetic ions Co^{2+} ($3d^7$, $e_u^4 t_{2u}^3$) and Mn^{2+} ($3d^5$, $e_u^2 t_{2u}^3$) in the A-site, the Heisenberg interactions such as the super-exchange interactions J_{A-Cr} between the NN spins S_{Cr} and S_A are requested to be considered. Hence, the LKDM model could predict the possible magnetic structure of ground state by the parameter $u = 4J_{Cr-Cr}S_{Cr}/3J_{A-Cr}S_A$ in ACr_2O_4, as, e.g., a Néel-type long-range configuration for $u \leq u_0 = 8/9$ and a ferrimagnetic long-range spiral spin order (SSO) for $u_0 < u < u'' = 1.298$ are stable. When $u > u''$, the locally unstable region may appear and the ferrimagnetic long-range SSO should be considered as a first approximation. Indeed, both $CoCr_2O_4$ and $MnCr_2O_4$ present the ferrimagnetic SSO that triggers the appearance of a small electric polarization along with the significant magnetoelectric coupling. $CoCr_2O_4$ ($MnCr_2O_4$) presents a magnetic phase transition to the collinear ferrimagnetic long-range order with an easy axis parallel to the [001] ($[1\bar{1}0]$) direction at $T_N \sim 95$ K (43 K), an incommensurate SSO at $T_S \sim 26$ K (19 K). In addition, another controversial SSO ground state appears at $T_L \sim 14$ K and 17 K for $CoCr_2O_4$ and $MnCr_2O_4$, respectively.[17–23] Several experimental works have estimated the features of magnetic structures of the ground states. As the reported single-crystal neutron diffraction and resonant soft x-ray magnetic scattering experiments in $CoCr_2O_4$, both commensurate [wave vector $\boldsymbol{q} \sim (2/3, 2/3, 0)$] and the incommensurate [$\boldsymbol{q} \sim (0.63, 0.63, 0)$] SSO were observed below T_L.[24,25] The slight change in $\boldsymbol{q}$ should be sensitive to the oxygen content originating from the synthetic conditions in different groups, which leads to the controversial magnetic ground state, short-range or long-range, and commensurate or incommensurate SSO. Based on our experimental observations, the synthesized $CoCr_2O_4$ in this work should exhibit the coexisting magnetic ground state, where the commensurate SSO is regarded as the main phase. However, they vary from the long-range to short-range SSO, corresponding to the different values of u.[26]

In this Letter, we investigate the structure and related dynamics of $CoCr_2O_4$ and $MnCr_2O_4$ by the x-ray diffraction (XRD), magnetization, heat capacity, and powder inelastic neutron scattering (INS) techniques. The INS spectra are analyzed by the Landau–Lifshitz–Gilbert (LLG) method,[27] and the exchange energies are deduced. Furthermore, the spin-phonon interaction and the quantum effect are discussed.

Experimental Details. The polycrystalline samples of ACr_2O_4 (A = Co and Mn)) were prepared by the solid-state reaction method. Stoichiometric amounts of Cr_2O_3 (99%, Alfa Aesar), Co_3O_4 (99.9%, Alfa Aesar) and MnO (99%, Alfa Aesar) powders were mixed in air and fully ground; then, the mixtures were pressed into thin cylindrical pellets with diameter of 10 mm, loaded in the alumina crucibles, and sintered at 1200° in air for 20 h. After thoroughly grinding the sintered mixture again, we repeated the above-mentioned operations and sintered at 1300° in air for 20 h. Finally, we successfully prepared the $CoCr_2O_4$ and $MnCr_2O_4$ polycrystalline samples.

Figures S1(a) and S1(b) in the Supplementary Material present the powder XRD data of $CoCr_2O_4$ and $MnCr_2O_4$, using Cu K_α source at room temperature. The structural Rietveld refinement profiles of the XRD data by FullProf software reveal the pure phase and cubic spinel structure with space group $Fd\bar{3}m$. The fitted results give the lattice parameters $a = 8.33106(0)$ Å for $CoCr_2O_4$ and $a = 8.43652(2)$ Å for $MnCr_2O_4$. The magnetization measurements were performed using a vibrating sample magnetometer in the physical properties measurement system (PPMS Dynacool-9 system, Quantum Design) with a field up to 9 T. The heat capacity measurements were carried out using the relaxation method by a PPMS Dynacool-9 system.

The inelastic neutron scattering measurements were carried out with the time-of-flight (TOF) spectrometer MARI, ISIS Neutron and Muon Source, Rutherford Appleton Laboratory. The incident neutron energies were selected as $E_i = 9$, 20, 75, and 150 meV using a Fermi chopper with a gadolinium slit pack running at 200 Hz (9, 20, 75 meV) and 300 Hz (150 meV). Approximately 5 g of powder samples of the $CoCr_2O_4$ and $MnCr_2O_4$ was loaded in an aluminum can. The measurements were performed at 5 K, 30 K, and 250 K with a top-loading closed-cycle He refrigerator. All TOF data were analyzed using the DAVE software.[28] Integrations of the TOF data over the range of momentum transfers $5 \leq Q \leq 16$ Å^{-1} and $E_i = 150$ meV were analyzed by getDOS programs[29] that lead to neutron-weighted phonon density of states (DOSs) for the $CoCr_2O_4$ and $MnCr_2O_4$ samples. In the following, we provide some results and discussions.

Phonon Density of States and Spin-Wave Excitations. When entering into the SSO state, both $CoCr_2O_4$ and $MnCr_2O_4$ present significant magnetoelectric coupling, which can be explained by two models, the inverse Dzyaloshinskii–Moriya (DM) or the spin-current model. Confusingly, the appearances of the magnetoelectric effect and the polarization reversal seem to be closely related to the synthesis conditions of $CoCr_2O_4$ and $MnCr_2O_4$. Specifically, the changes of the oxygen content could greatly weaken the magnetoelectric effect and even make it undetectable in $MnCr_2O_4$.[30] The oxygen content influences the Cr–Cr exchange interactions, which are dominant in the system and thus drive the observed physical phenomena. This phenomenon is also mapped in the Raman experiments, where only two Raman activity peaks centered at $E_g = 457$ cm^{-1} and $A_{1g} = 671$ cm^{-1} were observed, which deviate from theoretical expectations. In our previous work, we observed all Raman active modes as expected in the high-quality $MnCr_2O_4$ single crystals with almost perfect stoichiometric ratio.[30] A possible explanation for the observed different physical performance should be attributed to the competition among the main exchange interactions J_{Cr-Cr} and J_{A-Cr} of the $CoCr_2O_4$ and $MnCr_2O_4$.[31] The short Cr–Cr bonds of 2.9824 Å pro-

duce a strong AFM direct exchange interaction between *dd* orbitals, and the edge-shared CrO_6 octahedrons induce an indirect ferromagnetic 90° Cr–O–Cr super-exchange interaction mediated by O^{2-} p orbital. Such a balance between them leads to complex AFM exchange interactions J_{Cr-Cr}, which plays a dominant role in the origin of complex magnetism of ground state in the $CoCr_2O_4$ and $MnCr_2O_4$. Additionally, according to previous theoretical work, A–Cr exchange interactions cannot be neglected in spinel structures.[16] Hence, the changes of the oxygen content may affect the strength of the magnetic frustrations, leading to different experimental observations on the SSO and the magnetoelectric effect in the ground state.

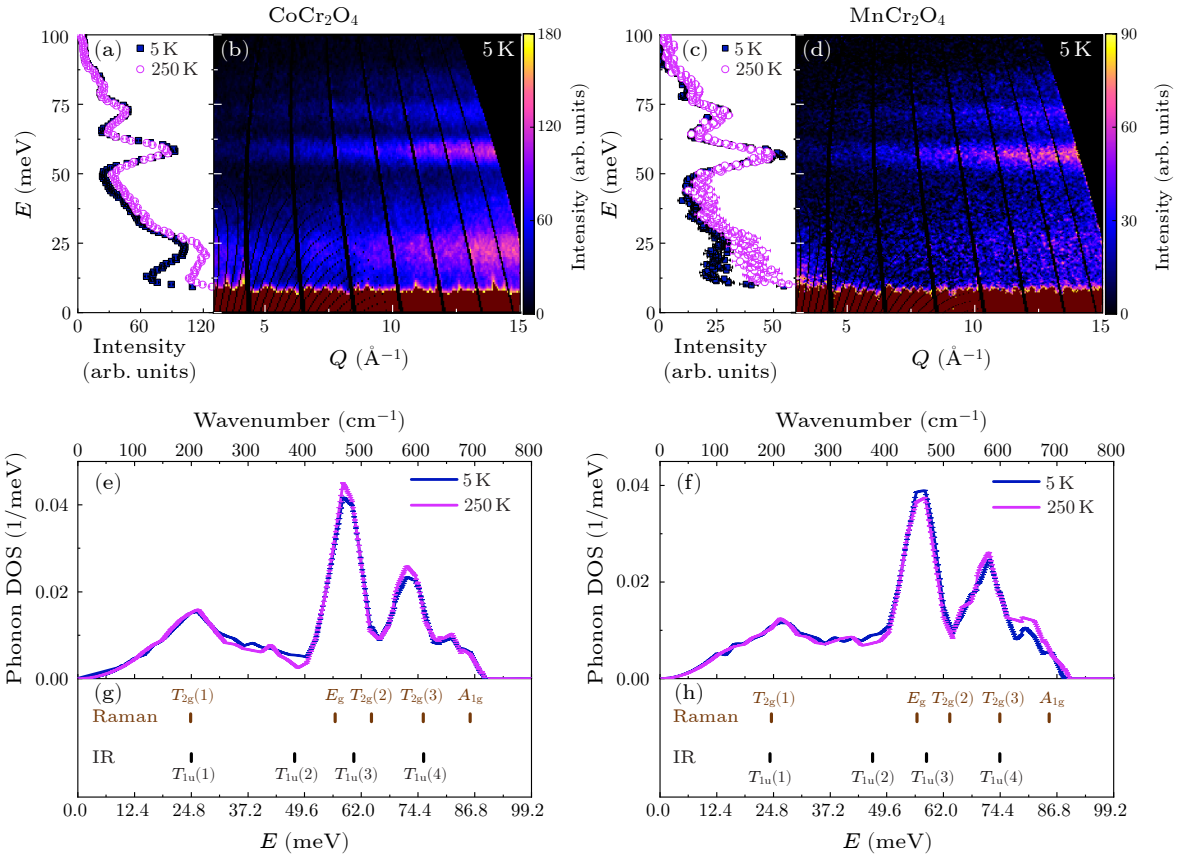

Fig. 1. [(a), (c)] The constant-Q cuts over the momentum ranges $Q = [5, 15]\,\text{Å}^{-1}$ for $CoCr_2O_4$ and $MnCr_2O_4$ powders. [(b), (d)] Experimental inelastic neutron scattering phonon excitations in the momentum Q and energy E space, collected by TOF spectrometer MARI with $E_i = 150\,\text{meV}$ at 5 K. The color bars indicate the scattering intensity on a linear scale. [(e), (f)] Neutron-weighted phonon density of states of $CoCr_2O_4$ and $MnCr_2O_4$ measured at 250 K and 5 K. [(g), (h)] The four infrared (IR)-active phonon modes and five Raman-active phonon modes of $CoCr_2O_4$ and $MnCr_2O_4$ measured at 10 K.[30,32,33]

Based on the above analyses, we performed powder INS experiments. As shown in Figs. 1(a) and 1(d), we begin with the phonon excitations. Figures 1(b) and 1(d) show the momentum and energy dependence of powder averaged dynamical structure factor $S(Q, E)$ of $CoCr_2O_4$ and $MnCr_2O_4$, respectively, at 5 K, as an example. The phonon excitations show the normal Q^2 dependence. For comparison, we plot the constant-Q cuts of the high-temperature paramagnetic state (250 K) and the SSO (5 K) together, Fig. 1(a) for $CoCr_2O_4$ and Fig. 1(c) for $MnCr_2O_4$, indicating the almost identical phonon excitations and maintaining the cubic structure in the whole temperatures as reported previously.[30] When integrating the $S(Q, E)$ over the range of momentum transfers $6 \le Q \le 15\,\text{Å}^{-1}$, we extract the neutron-weighted phonon DOSs by getDOS programs [see Figs. 1(e) and 1(f)]. Four phonon bands, located in the ranges of 0–37 meV, 37–65 meV, 65–78 meV, and 78–89 meV, are observed, corresponding to one acoustic phonon band and three optical phonon bands, respectively.

Although the exact lattice symmetry and the spin configuration of the magnetically ordered state are still subject of debate,[12,14,32,34] the dominant structural feature of the low-temperature phase is a tetragonal distortion with an elongation along [001] for $CdCr_2O_4$[35] and a contraction for $ZnCr_2O_4$[15] and $MgCr_2O_4$.[34] Given these significant structural changes at low temperatures, we attempted an estimate based on the analogy with $ZnCr_2O_4$ to understand the temperature dependence of $CoCr_2O_4$ and $MnCr_2O_4$, even though the phonon frequencies and the local lattice symmetry of $ZnCr_2O_4$ are not exactly matched with those of $CoCr_2O_4$ and $MnCr_2O_4$. According to the phonon calculation for $ZnCr_2O_4$ at room temperature, it is reasonable to consider that the $200\,\text{cm}^{-1}$

mode frequencies of $CoCr_2O_4$ and $MnCr_2O_4$ are determined mainly from force constants of Co–O and Mn–O vibration. The 457 cm^{-1} mode frequencies can be determined mainly from the force constants of Cr–Cr and Cr–O vibrations. The 671 cm^{-1} mode frequencies are mostly influenced by the force constants of Cr–O vibration.

A careful comparison of the neutron-weighted phonon DOSs in Figs. 1(e) and 1(f) shows that the optical phonon bands exhibit clear changes at 250 K and 5 K. In $ZnAl_2O_4$, O motions are well localized near the end of the phonon spectra, with a sharp peak around 800 cm^{-1} composed almost entirely of oxygen vibrations.[36] In comparison with $MnCr_2O_4$, we observe significant changes in the phonon spectra at 671 cm^{-1} between 5 K and 250 K, which may be highly correlated with oxygen vibrations. However, the phonon spectra of $CoCr_2O_4$ do not exhibit similar characteristics, showing consistency between 5 K and 250 K. Notably, in the previously reported $CoCr_2O_4$, the ground state presents a coexistence of commensurate SSO and ferroelectric order.[37] In contrast, $MnCr_2O_4$ shows no multiferroicity.[15,30,33] One possible reason for this difference is that the SSO in $MnCr_2O_4$ is highly sensitive to the oxygen concentration. The observed changes in the phonon spectra, especially regarding O motions, offer an additional insight into the correlation between oxygen content and the SSO as well as the magnetoelectric effect in the ground state of $MnCr_2O_4$.

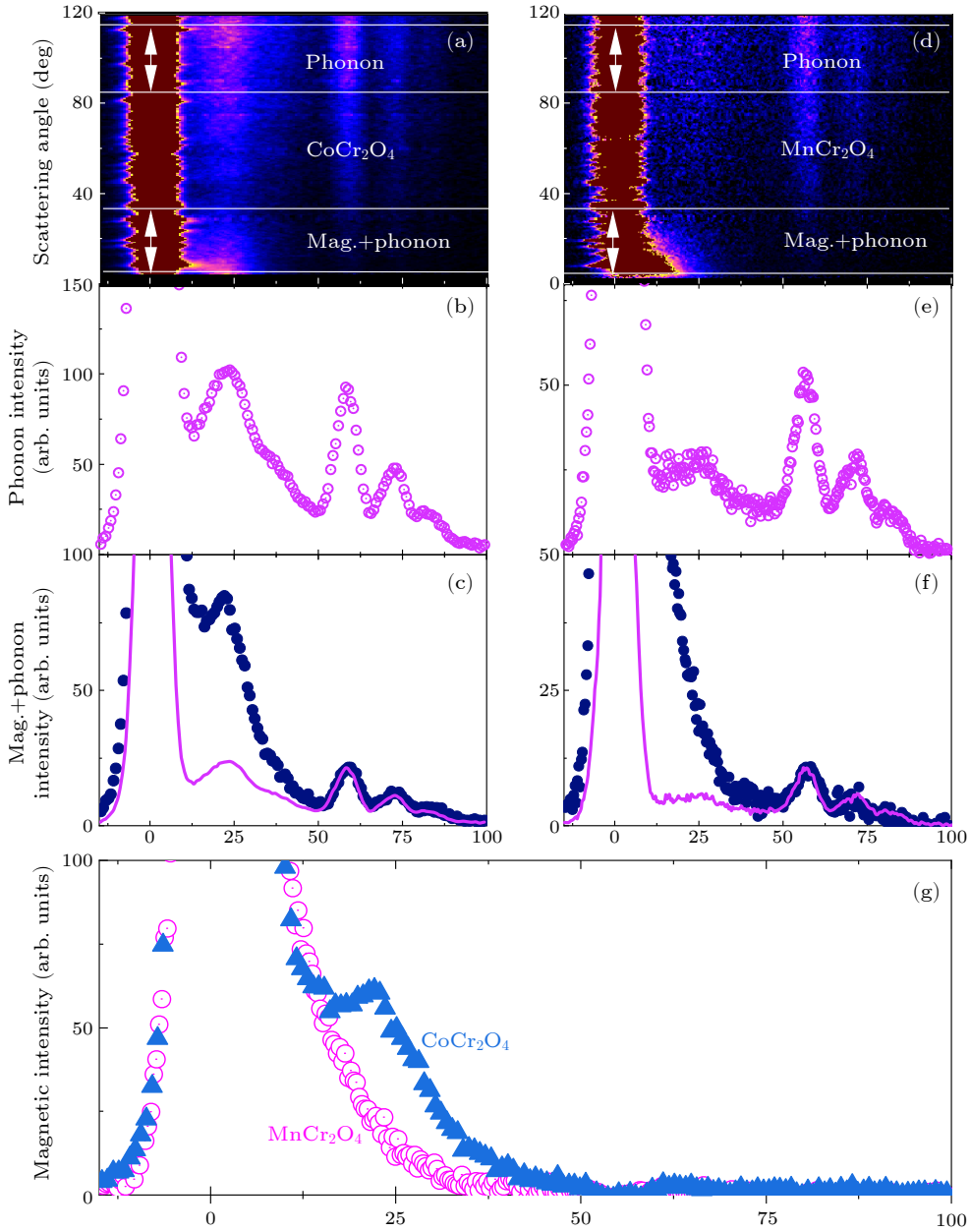

Fig. 2. [(a), (d)] Inelastic neutron scattering intensity of (a) $CoCr_2O_4$ and (d) $MnCr_2O_4$ (color scale) versus Q and energy transfer at $T = 5$ K and $E_i = 150$ meV, respectively. Horizontal white lines delineate regions where phonon and magnetic scattering are isolated. [(b), (e)] Neutron intensity summed over the high-angle range 85°–115° originating mainly from phonons. [(c), (f)] Neutron intensity summed over the low angle range 5°–35° (dark blue circles) and phonon background scaled from high angle sum (purple solid lines). (g) Isolated magnetic scattering at $T = 5$ K.

Figure 2(a) presents the comprehensive spectra for $CoCr_2O_4$ at $T = 5\,K$ as functions of 2θ and $\hbar\omega$. The data clearly distinguish between phonon and magnetic scattering regions, with horizontal white lines delineating these zones. Figure 2(b) shows the phonon scattering by summing the neutron intensity over the high-angle range ($2\theta = 85°$–$115°$). This range mainly captures the phonon contributions because the effect of magnetic scattering is smaller at higher Q values, where the magnetic form factor decreases. The resulting phonon spectra provide a clear picture of the lattice dynamics without the interference of magnetic excitations. Conversely, Fig. 2(c) sums the neutron intensity over the low-angle range ($2\theta = 5°$–$35°$), capturing both phonon and spin wave contributions. By subtracting the high-angle data (phonon scattering) from the low-angle data, we isolate the magnetic scattering component. This subtraction, scaled by a constant factor, reveals the pure magnetic scattering profile.

In the difference plot shown in Fig. 2(g), the strong peak at 0 meV represents elastic scattering, which includes both nuclear and magnetic contributions that cannot be distinguished using the difference method. A distinct peak at ~ 25 meV indicates the resulting magnetic intensity for $CoCr_2O_4$ after the subtraction process. In contrast, the signal for $MnCr_2O_4$ displays a noticeable broadening around 20 meV. This broadening may originate from the effects of high frustration as mentioned in the susceptibility result given in the Supplementary Material and quantum fluctuations.

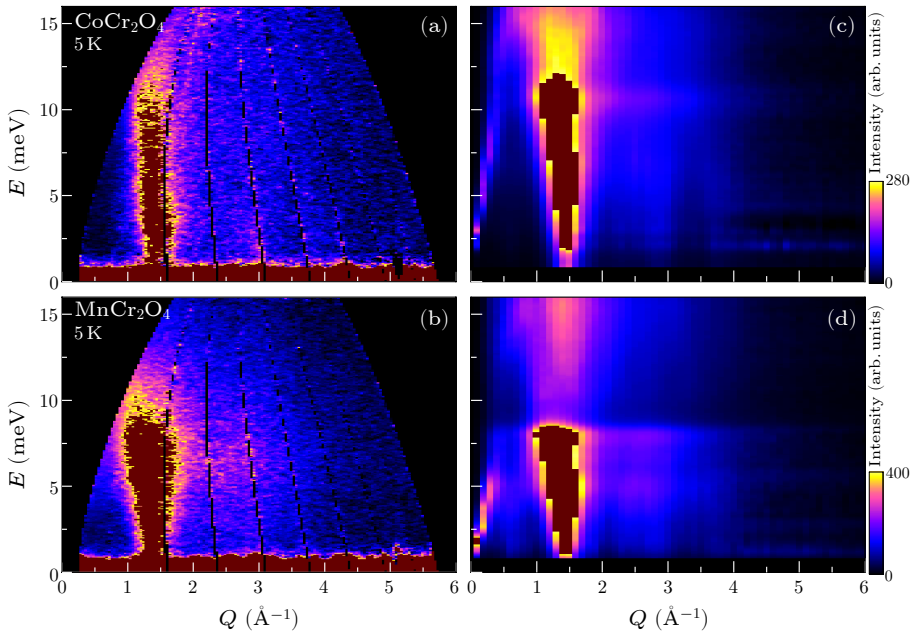

Fig. 3. Inelastic neutron scattering results for $CoCr_2O_4$ and $MnCr_2O_4$ at 5 K with an incident energy E_i of 20 meV. [(a), (b)] Experimental inelastic neutron scattering spectra for $CoCr_2O_4$ and $MnCr_2O_4$, respectively. [(c), (d)] Calculated excitation spectra using the LLG method for $CoCr_2O_4$ and MnCr2O4, respectively. The calculations were performed using the parameters listed in Table 1.

Both observed and calculated intensities at 5 K are displayed as two-dimensional plots in Fig. 3. The inelastic neutron scattering results for $CoCr_2O_4$ and $MnCr_2O_4$ at 5 K with an incident energy E_i of 20 meV reveal distinct differences in the excitation spectra of these spinel compounds. Figures 3(a) and 3(b) present the experimental data, which display clear features corresponding to the magnetic excitations. In $CoCr_2O_4$, the spectra show a prominent spin wave excitation centered around 1.4 $Å^{-1}$ with excitations extending up to 15 meV. $MnCr_2O_4$ exhibits a similar structure but with broader and less-intensity features, indicating differences in their magnetic interactions. The differences in the excitation spectra could be influenced by the different magnetic anisotropies and spin-orbit coupling effects in these materials.[32,38–40] The broader excitations in $MnCr_2O_4$ might result from greater magnetic frustration as mentioned in the susceptibility measurement or weaker exchange interactions, leading to a less well-defined magnetic structure.

To better understand these excitations, we performed calculations using the LLG method. We focus on fitting the excitation at $Q = 1.4\,Å^{-1}$ as shown in Fig. 3. These calculations were based on the Heisenberg model only considering the NN AFM exchange interactions, so that the Hamiltonian can be defined as follows:

$$H = J_{BB} \sum_{\langle i,j \rangle} S_{Bi} \cdot S_{Bj} + J_{AB} \sum_{\langle i,j \rangle} S_{Ai} \cdot S_{Bj} + J_{AA} \sum_{\langle i,j \rangle} S_{Ai} \cdot S_{Aj}. \quad (1)$$

Using classical Monte Carlo simulations, initial spin configurations were generated on a $10 \times 10 \times 10$ supercell of conventional cubic cells and 5×10^4 single-spin Metropolis updates were applied. To reduce autocorrelation, overrelaxation sweeps were introduced after each Monte Carlo

sweep. The equation of motion of the spins was calculated using Verner's "Most Efficient" 7/6 Runge-Kutta method, in which spin configurations were evolved over 800 steps,[41] with a step size of $\tau = 1/J$. The spin excitation spectra were obtained through a fast Fourier transform. For improved statistical accuracy, 1000 random numbers were used in the simulation of powder averaging results, and $S(Q, \omega)$ was averaged across roughly 10 independent simulations. Additionally, a classical statistical factor $\omega/(2k_BT)$ was applied to $S(Q, \omega)$ to compare with the experimental data.[42]

Table 1. Ferrimagnetic parameters obtained from the fitting of the susceptibility with Eq. (1) in the Supplementary Material, including the Curie constant (C), Weiss temperature (θ), correction factor (ζ), modified Curie–Weiss temperature (θ'), effective magnetic moment (μ_{eff}), and the ratio $|\theta|/T_C$. Values of the ionic spin, exchange parameters, and the dimensionless parameter u calculated for $CoCr_2O_4$ and $MnCr_2O_4$. The parameter u is defined according to the LKDM theory and is given by $u = 4J_{Cr-Cr}S_{Cr}/3J_{A-Cr}S_A$.

	$CoCr_2O_4$	$MnCr_2O_4$
S_A	3/2	5/2
S_{Cr}	3/2	3/2
C(emu·K/mol)	5.86	8.80
θ (K)	−600.1	−425.0
Z (mol·K/emu)	1085.0	1338.6
θ' (K)	88.9	24.5
$\mu_{\text{eff}}(\mu_B)$	6.85	8.39
$f = \|\theta\|/T_C$	6.32	9.88
J_{Cr-Cr} (meV)	0.48	0.44
J_{A-Cr} (meV)	0.22	0.18
J_{A-A} (meV)	0.03	0.03
$u(4J_{Cr-Cr}S_{Cr}/3J_{A-Cr}S_A)$	2.91	1.96

The theoretical calculations, as shown in Figs. 3(c) and 3(d), provide a good match to the experimental data, capturing the essential characteristics of the magnetic excitations, thus providing a clearer way to understand the spin dynamics in these materials. In $CoCr_2O_4$ [Fig. 3(c)], the calculated spectra replicates the experimental spin wave excitation around 1.4 Å^{-1}, while for $MnCr_2O_4$ [Fig. 3(d)], the calculations reflect the broader distribution of excitations observed experimentally. However, some details show that our classical model cannot fully describe the behavior of the system, thus indicating the presence of quantum effects.

Table 1 lists the exchange interactions J_{Cr-Cr}, J_{A-Cr}, and J_{A-A}, as well as the parameter u, calculated by $u = 4J_{Cr-Cr}S_{Cr}/3J_{A-Cr}S_A$ according to the LKDM theory. For both $CoCr_2O_4$ and $MnCr_2O_4$, the values of u fall outside the range typically associated with a stable ground state. Specifically, the u value for $CoCr_2O_4$ is 2.91, while for $MnCr_2O_4$, it is 1.96. This further indicates the limitations of the classical model.

In summary, we have performed bulk characterization of magnetization and specific heat, demonstrating that $CoCr_2O_4$ undergoes a first-order phase transition. This is evidenced by the latent heat near T_S and the thermal hysteresis in the C_P(T) curve near T_L. From inelastic neutron scattering experiments, the neutron-weighted phonon density of states is obtained and the relationship between oxygen vibrations and SSO through significant changes are observed at 250 K and 5 K. By separating the phonon and magnetic signals, we observe the broadening of the magnetic signal in $MnCr_2O_4$ from the geometric frustration and quantum fluctuations. We combine the measured spin wave excitations in $CoCr_2O_4$ and $MnCr_2O_4$ with calculations based on the Heisenberg model to determine the exchange energy of the system. The result provides evidence of the existence of quantum effect in the ground state and a comprehensive understanding of spin dynamics and magnetic interactions. Exploring the quantum effect on the ground state of a frustrated magnet is very challenging: usually the broadening spin dynamics is a signal of strong quantum effect, however, the broadening signal has been reported in a high-spin Mn-oxide($S = 5/2$) with a triangular lattice recently;[43] in addition, the applied direction of the external field could adjust the interactions and induce different magnetic states.[44] Future investigations with extra factors may help to elucidate those novel properties, potentially leading to new insights into the quantum behavior.[45]

Acknowledgements. W. X., G. L., M. S., J. J., and J. M. thank the financial support from the National Key Research and Development Program of China (Grant No. 2022YFA1402702), the National Science Foundation of China (Grant Nos. U2032213 and 12004243), the Interdisciplinary Program of Wuhan National High Magnetic Field Center (Grant No. WHMFC 202122), Huazhong University of Science and Technology. Q. R. acknowledged the support from the National Natural Science Foundation of China (Grant No. 52101236), Guangdong Basic and Applied Basic Research Foundation (Grant No. 2021B1515140014), and the Guangdong Provincial Key Laboratory of Extreme Conditions. X. L. and Y. P. Sun thank financial support from the National Key Research and Development Program of China (Grant Nos. 2021YFA1600201 and 2023YFA1607402), the National Science Foundation of China (Grant No. 12274412). H.Z. thanks the support of NSF-DMR-2003117. Experiments at the ISIS Neutron and Muon Source were supported by a beamtime allocation RB1910163 from the Science and Technology Facilities Council. Data is available at https://doi.org/10.5286/ISIS.E.RB1910163.

References

[1] Moessner R and Chalker J T 1998 *Phys. Rev. Lett.* **80** 2929
[2] Bai X, Paddison J A M, Kapit E, Koohpayeh S M, Wen J J, Dutton S E, Savici A T, Kolesnikov A I, Granroth G E, Broholm C L, Chalker J T, and Mourigal M 2019 *Phys. Rev. Lett.* **122** 097201
[3] Tymoshenko Y V, Onykiienko Y A, Müller T, Thomale R, Rachel S, Cameron A S, Portnichenko P Y, Efremov D V, Tsurkan V, Abernathy D L, Ollivier J, Schneidewind A, Piovano A, Felea V, Loidl A, and Inosov D S 2017 *Phys. Rev. X* **7** 041049
[4] Gao S, Guratinder K, Stuhr U, White J S, Mansson M, Roessli B, Fennell T, Tsurkan V, Loidl A, Ciomaga Hatnean M, Balakrishnan G, Raymond S, Chapon L, Garlea

V O, Savici A T, Cervellino A, Bombardi A, Chernyshov D, Rüegg C, Haraldsen J T, and Zaharko O 2018 *Phys. Rev. B* **97** 134430
[5] Lee S H, Broholm C, Ratcliff W, Gasparovic G, Huang Q, Kim T H, and Cheong S W 2002 *Nature* **418** 856
[6] Glazkov V N, Farutin A M, Tsurkan V, von Nidda H A K, and Loidl A 2009 *J. Phys.: Conf. Ser.* **145** 012030
[7] Matsuura K, Sagayama H, Uehara A, Nii Y, Kajimoto R, Kamazawa K, Ikeuchi K, Ji S, Abe N, and Arima T H 2017 *Phys. Rev. Lett.* **119** 017201
[8] Ma J, Lee J H, Hahn S E, Hong T, Cao H B, Aczel A A, Dun Z L, Stone M B, Tian W, Qiu Y, Copley J R D, Zhou H D, Fishman R S, and Matsuda M 2015 *Phys. Rev. B* **91** 020407
[9] Lee J H, Ma J, Hahn S E, Cao H B, Lee M, Hong T, Lee H J, Yeom M S, Okamoto S, Zhou H D, Matsuda M, and Fishman R S 2017 *Sci. Rep.* **7** 17129
[10] Jiao J L, Zhang H P, Huang Q, Wang W, Sinclair R, Wang G, Ren Q, Lin G T, Huq A, Zhou H D, Li M Z, and Ma J 2021 *J. Phys.: Condens. Matter* **33** 134002
[11] Chung J H, Kim J H, Lee S H, Sato T J, Suzuki T, Katsumura M, and Katsufuji T 2008 *Phys. Rev. B* **77** 054412
[12] Kiswandhi A, Ma J, Brooks J S, and Zhou H D 2014 *Phys. Rev. B* **90** 155132
[13] Ma J, Garlea V O, Rondinone A, Aczel A A, Calder S, dela Cruz C, Sinclair R, Tian W, Chi S, Kiswandhi A, Brooks J S, Zhou H D, and Matsuda M 2014 *Phys. Rev. B* **89** 134106
[14] Glazkov V N, Farutin A M, Tsurkan V, von Nidda H A K, and Loidl A 2009 *Phys. Rev. B* **79** 024431
[15] Kemei M C, Barton P T, Moffitt S L, Gaultois M W, Kurzman J A, Seshadri R, Suchomel M R, and Kim Y I 2013 *J. Phys.: Condens. Matter* **25** 326001
[16] Kaplan T A, Dwight K, Lyons D, and Menyuk N 1961 *J. Appl. Phys.* **32** S13
[17] Dey K, Majumdar S, and Giri S 2014 *Phys. Rev. B* **90** 184424
[18] Yoon D Y, Lee S, Oh Y S, and Kim K H 2010 *Phys. Rev. B* **82** 094448
[19] Tomiyasu K, Fukunaga J, and Suzuki H 2004 *Phys. Rev. B* **70** 214434
[20] Hastings J M and Corliss L M 1962 *Phys. Rev. B* **126** 556
[21] Sinclair R, Ma J, Cao H B, Hong T, Matsuda M, Dun Z L, and Zhou H D 2015 *Phys. Rev. B* **92** 134410
[22] Kitani S, Tachibana M, Taira N, and Kawaji H 2013 *Phys. Rev. B* **87** 064402
[23] Bordács S, Varjas D, Kézsmárki I, Mihály G, Baldassarre L, Abouelsayed A, Kuntscher C A, Ohgushi K, and Tokura Y 2009 *Phys. Rev. Lett.* **103** 077205
[24] Chang L J, Huang D J, Li W H, Cheong S W, Ratcliff W, and Lynn J W 2009 *J. Phys.: Condens. Matter* **21** 456008
[25] Windsor Y W, Piamonteze C, Ramakrishnan M, Scaramucci A, Rettig L, Huever J A, Bothschafter E M, Bingham N S, Alberca A, Avula S R V, Noheda B, and Staub U 2017 *Phys. Rev. B* **95** 224413
[26] Ederer C and Komelj M 2007 *Phys. Rev. B* **76** 064409
[27] Zhang S F and Zhang S S L 2009 *Phys. Rev. Lett.* **102** 086601
[28] Azuah R T, Kneller L R, Qiu Y M *et al.* 2009 *J. Res. Natl. Inst. Stand. Technol.* **114** 341
[29] Budai J D, Hong J, Manley M E, Specht E D, Li C W, Tischler J Z, Abernathy D L, Said A H, Leu B M, Boatner L A, McQueeney R J, and Delaire O 2014 *Nature* **515** 535
[30] Lin G T, Wang Y Q, Luo X, Ma J, Zhuang H L, Qian D, Yin L H, Chen F C, Yan J, Zhang R R, Zhang S L, Tong W, Song W H, Tong P, Zhu X B, and Sun Y P 2018 *Phys. Rev. B* **97** 064405
[31] Tomiyasu K, Suzuki H, Toki M, Itoh S, Matsuura M, Aso N, and Yamada K 2008 *Phys. Rev. Lett.* **101** 177401
[32] Kocsis V, Bordács S, Varjas D, Penc K, Abouelsayed A, Kuntscher C A, Ohgushi K, Tokura Y, and Kézsmárki I 2013 *Phys. Rev. B* **87** 064416
[33] Sethi A, Byrum T, McAuliffe R D, Gleason S L, Slimak J E, Shoemaker D P, and Cooper S L 2017 *Phys. Rev. B* **95** 174413
[34] Ortega-San-Martín L, Williams A J, Gordon C D, Klemme S, and Attfield J P 2008 *J. Phys.: Condens. Matter* **20** 104238
[35] Kimura S, Sawada Y, Narumi Y, Watanabe K, Hagiwara M, Kindo K, and Ueda H 2015 *Phys. Rev. B* **92** 144410
[36] Fang C M, Loong C K, de Wijs G A, and de With G 2002 *Phys. Rev. B* **66** 144301
[37] Pardo-Sainz M, Toshima A, André G, Basbus J, Cuello G J, Laliena V, Honda T, Otomo T, Inoue K, Hosokoshi Y, Kousaka Y, and Campo J 2023 *Phys. Rev. B* **107** 144401
[38] Mufti N, Nugroho A A, Blake G R, and Palstra T T M 2010 *J. Phys.: Condens. Matter* **22** 075902
[39] McQueeney R J, Yan J Q, Chang S, and Ma J 2008 *Phys. Rev. B* **78** 184417
[40] Ma J, Yan J Q, Diallo S O, Stevens R, Llobet A, Trouw F, Abernathy D L, Stone M B, and McQueeney R J 2011 *Phys. Rev. B* **84** 224115
[41] Verner J H 2010 *Numer. Algorithms* **53** 383
[42] Pohle R, Yan H, and Shannon N 2021 *Phys. Rev. B* **104** 024426
[43] Shu M, Dong W, Jiao J, Wu J, Lin G, Kamiya Y, Hong T, Cao H, Matsuda M, Tian W, Chi S, Ehlers G, Ouyang Z, Chen H, Zou Y, Qu Z, Huang Q, Zhou H, and Ma J 2023 *Phys. Rev. B* **108** 174424
[44] Lin G, Shu M, Zhao Q, Li G, Ma Y, Jiao J, Li Y, Duan G, Huang Q, Sheng J, Kolesnikov A I, Li L, Wu L, Chen H, Yu R, Wang X, Liu Z, Zhou H, and Ma J 2024 *Innovat. Mater.* **2** 100082
[45] Ma J 2023 *Nat. Phys.* **19** 922